Identifying parameters of nonlinear structural dynamic systems using linear time-periodic approximations

Michael W. Sracic
Graduate Research Assistant, Ph.D Candidate
mwsracic@wisc.edu
&
Matthew S. Allen
Assistant Professor
msallen@engr.wisc.edu
Department of Engineering Physics
University of Wisconsin-Madison
534 Engineering Research Building
1500 Engineering Drive
Madison, WI 53706

ABSTRACT

While numerous mature parametric identification methods are available for linear systems, there are only a few methods capable of identifying parametric models for multiple degree of freedom nonlinear systems. In a previous work, the authors proposed a new identification routine for nonlinear systems based on harmonically forcing a system in a periodic orbit and then recording deviations from that orbit. Under mild assumptions one can model the response about the periodic orbit using a linear time-periodic system model that is relatively easy to identify from the measurements using a variety of techniques. The method provides an estimate of the time periodic state coefficient matrix of the system which gives direct information on the order of the system and the nonlinear-parameters. A prior work explored the method in detail for a single degree-of-freedom system, but it has only been applied to an MDOF system with a limited set of excitation conditions. This work explores a range of possible excitation signals using an analytical model of a cantilever beam with a cubic spring at its tip. Numerical continuation techniques are used to find the stable and unstable periodic responses of the beam and different excitation strategies are explored. Additionally, the method is validated on the analytical model with a conventional approach for nonlinear system identification. The most promising strategies are then applied to a real beam with a significant geometric nonlinearity.

1.   Introduction

Most dynamical systems behave nonlinearly in the most general scenario. This can be observed in various structural dynamic systems such as an airplane wing that flutters wildly near a stall point bifurcation [1], in rotor dynamic systems with bearing contact nonlinearities [2], in biomechanics systems such as the human body which has muscles that produce nonlinear forces that move joints through large angles [3-5], or in social science systems such as psychology [6] and economics [7]. While many techniques are available to extract linear time-invariant mathematical models from experimental measurements of these systems, the linear models cannot correctly characterize some of the complex nonlinear phenomena exhibited. Therefore, nonlinear models are needed and nonlinear identification methods are required to extract the nonlinear models from measurements.

A few methods for experimental identification are currently available. Some notable time domain techniques have been successfully applied experimentally such as the restoring force surface method [8], the Hilbert and Huang-Hilbert transforms [9], and the NARMAX method [10]. The former three methods cannot be easily applied to higher order systems while the latter method requires one to assume a form for the nonlinearity in the system prior to the identification. The notable frequency domain techniques consist of the Volterra and Weiner series techniques, the Conditioned Reverse Path method, and the Nonlinear Identification through Feedback of the Output method, all of which were reviewed in [10]. The Volterra and Weiner series techniques require very large amounts of data for even low order nonlinearities. The other two methods

require one to first assume a form of the nonlinearity. A nonlinear normal-modal based technique has also been proposed and is currently being investigated [10, 11].

The authors recently proposed an alternative to these approaches that may overcome some of these limitations. It is a frequency domain technique [12] based on spectra that are similar to linear frequency response functions. Because of this similarity, it allows many concepts from linear system identification to be applied to nonlinear systems and the analyst can distinguishthe features in the spectra that are due the nonlinear response rather than measurement noise. The method provides direct information on the order of the system, the nonlinear parameters, and does not require an a priori assumption regarding the form of the nonlinearities. The basic idea is to drive the nonlinear system so that it responds in a stable periodic orbit and then to perturb the system slightly from the periodic orbit. If the nonlinearities are sufficiently smooth and the deviations from the periodic orbit are sufficiently small, the resulting response can be well approximated with a linear time-periodic model. A number of techniques are then available for identifying a linear time-periodic model for the system. This work utilizes the *Lifting* and *Fourier Series Expansion* (FSE) methods, which were both proposed by Allen in [13]. These techniques are appealing because the linear time-periodic response can be shown to be mathematically equivalent to the response of an augmented linear time invariant system. Therefore, a linear time-invariant parameter extraction method can be used to estimate the linear time-periodic system model, making this parameter estimation step quite convenient. The linear time-periodic model is used to construct the state transition matrix and state coefficient matrix for each state along the original periodic orbit. Finally, the constructed state coefficient matrix can be used to calculate an estimate of the nonlinear system parameters.

The original work by the authors [14] verified the method on simulated measurements of a second order analytical Duffing oscillator, and some original efforts were made to apply the method to a fourth order analytical nonlinear cantilever beam [12]. This work more thoroughly explores the performance of the method for systems with multiple degrees of freedom, and also applies the method to real experimental measurements of a high order system. The experimental system consists of a cantilever beam with a strip of spring steel connected between its free end and a fixture. The spring steel provides a geometric stiffening nonlinearity. The measurements are probed and found to contain clear evidence of time-periodic effects that are distinguishable from noise. A few different harmonic forcing conditions are considered and the state coefficient matrix is estimated, revealing the level of accuracy that is required to obtain meaningful results. Furthermore, in all of the preceding works the authors identified the periodic limit cycle but then used it only to define the state of the system. However, the limit cycle itself is strongly dependent on the nonlinear dynamic model for the system and could be used to perform nonlinear identification with a conventional algorithm. This work explores this possibility, using a variant on the restoring force surface method to compute the net nonlinear restoring force on each mass. That restoring force is then used to validate the results of the more detailed model that is found using the proposed linear time-periodic approximation. The following section provides the background theory that supports the technique. Then Section 3introduces the nonlinear beam for the experimental setup and the analytical model and applies the identification to simulated and experimental measurements of the beam. The results are presented and discussed, and finally some conclusions are provided.

2. Theory

2.1 Linear Time-Periodic Approximations of Nonlinear Systems

Generally, a forced nonlinear system can be represented in state space with the following equation

$$\dot{x} = f\left(x,u\right)$$
$$y = h\left(x,u\right)$$

(1)

where f and h are functions that describe how the time-dependent state of the system, $x(t)$, and the time-dependent inputs applied to the system, $u(t)$, influence the dynamics of the system. Assuming that the system has a periodic solution $\bar{x}\,(t+T)=\bar{x}\,(t)$, then one can define a periodic orbit γ, which is a trajectory in the state space that contains the state $\bar{x}$ for every time t. If a small input is applied to perturb the system from γ, then the state and input of the system can be described as small deviations from the periodic orbit, $x = \bar{x} + \tilde{x}$ and $u = \bar{u} + \tilde{u}$. If the nonlinearities are C^1 (at least one time continuously differentiable), then eq. 1 can be expanded in a Taylor series, and if the perturbation is sufficiently small the higher order terms can be neglected to obtain the following.

$$\dot{\tilde{x}} = \left[\partial f_i / \partial x_j\right]\Big|_{\overline{x} \in \gamma} \tilde{x} + \left[\partial f_i / \partial u_j\right]\Big|_{\overline{u}} \tilde{u}$$

$$\tilde{y} = \left[\partial h_i / \partial x_j\right]\Big|_{\overline{x} \in \gamma} \tilde{x} + \left[\partial h_i / \partial u_j\right]\Big|_{\overline{u}} \tilde{u}$$

(2)

The shorthand notation $\left[\partial f_i / \partial x_j\right]$ is used for the partial derivative matrices meaning that the component in the ith-row and j^{th}-column is the partial derivative of the ith component of f with respect to the jth component of x. Generally, the these matrices may depend on both x and u and would need to be evaluated at both $\overline{x}$ and $\overline{u}$, but typical structural dynamic systems do not contain this type of cross coupling. The approximate model given by the previous equation is that of a linear time-periodic state space system with $A(t) = \left[\partial f_i / \partial x_j\right]$, $B(t) = \left[\partial f_i / \partial u_j\right]$, $C(t) = \left[\partial h_i / \partial x_j\right]$, and $D(t) = \left[\partial h_i / \partial u_j\right]$. The solution of such a system is governed by the state transition matrix $\Phi(t, t_0)$, which transfers the state of the system from an initial time t_0 to time t. For this work, the disturbance force is impulsive such that $\tilde{u} = 0$ after the impulse. Then, the solution to eq. (2) is given by the following equation.

$$\tilde{x} = \Phi(t, t_0)\tilde{x}_0$$

$$\tilde{y} = C(t)\Phi(t, t_0)\tilde{x}_0$$

(3)

2.2   Review of System Identification Methods for Linear Time-Periodic Systems

When a system is well approximated as linear time-periodic without any degenerate modes, its state transition matrix can be represented using Floquet theory [13, 15-17] in summation form as

$$\Phi(t, t_0) = \sum_{r=1}^{n} \left[R(t)\right]_r e^{\lambda_r(t-t_0)}$$

$$\left[R(t)\right]_r = \{\phi(t)\}_r \{\eta(t_0)\}_r^{\mathrm{T}}$$

(4)

where n is the order of the system and $[R(t)]_r$ is the rth residue matrix corresponding to the rth Floquet exponent, λ_r, and is composed of the product of the rth time-periodic right Floquet eigenvector $\{\phi(t)\}_r$ and r^{th} constant left Floquet eigenvector $\{\eta(t_0)\}_r$ of the state transition matrix. Allen has suggested two techniques for extracting a model from such a system. The first is called the Fourier Series Expansion technique and the second is called the Lifting technique, and both result in a representation of the response that is linear time-invariant. The methods are summarized briefly here and are provided with further details in [13].

2.2.1   Fourier Series Expansion Technique

The residue matrix $[R(t)]_r$ in the previous equation is periodic because of the periodicFloquet eigenvectors $\{\phi(t)\}_r$ and can therefore be expanded in a Fourier series. After exchanging the order of summation and simplifying terms, the result is

$$\Phi(t, t_0) = \sum_{r=1}^{n} \sum_{m=-N_B}^{N_B} \left[B_m\right]_r e^{(\lambda_r + im\omega_T)(t-t_0)}$$

(5)

where $[B_m]_r$ is the mth Fourier coefficient matrix of the rth mode and $\omega_T = 2\pi/T$ is the period frequency. To be exact, the Fourier expansion must include an infinite number of terms, but in practice a finite number of Fourier terms, $m=-N_B,...,N_B$, will sufficiently approximate the expansion [12, 13]. The Fourier Series Expansion representation of the response is equivalent to a linear modal model with $n*(2*N_B+1)$ eigenvalues $\lambda_r + im\omega_T$.

2.2.2   Lifting technique

If the measured response of a time-periodic system is resampled at an integer number of points per period T, then an analysis can be performed based on "lifting" augmented signals from the full linear time-periodic response. Suppose that the response $y(t)$ has been sampled M times per period for an integer N_c cycles of the fundamental period. The lifted response y_m^l is the vector such that

$$y_m^l = \left[y_0^{\mathrm{T}}, y_1^{\mathrm{T}}, \cdots, y_{M-1}^{\mathrm{T}} \right]^{\mathrm{T}} \tag{6}$$

where y_k for $k=0,..,M$-1 is the response vector at t_j with $j=k+mM$ and m ranges from 0 to N_c-1 [13]. In the absence of an input force the lifted response can be arranged as

$$y_m^l = \sum_{r=1}^n \left\{ R^{ld} \right\}_r e^{\lambda_r mT} \tag{7}$$

where $\{R^{ld}\}_r$ is the residue vector of size M times the number of outputs of the response. One should note that $\{R^{ld}\}_r$ must account for the delay between the initial time and the kth time instant as discussed in [13]. The advantage of this approach is that the lifted response retains the order of the original linear time-periodic system. The eigenvalues may be aliased, but the aliased eigenvalues still provide a valid representation for the linear time-periodic system.

2.2.3   Constructing the System Model from Experimental Measurements

In [13], Allen discusses how the state transition matrix can be constructed from either of the models above assuming that one has measured the displacement of the system. The state vector of such a system consists of the measured displacement states as well as the corresponding velocity states, but the velocities are not typically measured, so Allen differentiated the Fourier Series Expansion model of the system to find the velocity states needed to form the state vector of the system. In this work, acceleration measurements are considered. When this is the case, the Fourier series expansion model for the free acceleration response is written as

$$x_a = \sum_{r=1}^N \sum_{m=-N_B}^{N_B} \left\{ B_m \right\}_r e^{(\lambda_r + im\omega_T)(t-t_0)} \tag{8}$$

where N is the number of degrees of freedom and $\{B_m\}_r$ is the residue vector. In order to create a full state vector that consists of N position states x_d and N velocity states x_v, one can integrate the previous equation two times successively to calculate the velocity and position states.

$$x_v = \sum_{r=1}^N \sum_{m=-N_B}^{N_B} \left\{ B_m \right\}_r \left(\lambda_r + im\omega_T \right)^{-1} e^{(\lambda_r + im\omega_T)(t-t_0)}$$

$$x_d = \sum_{r=1}^N \sum_{m=-N_B}^{N_B} \left\{ B_m \right\}_r \left(\lambda_r + im\omega_T \right)^{-2} e^{(\lambda_r + im\omega_T)(t-t_0)} \tag{9}$$

Then, the state transition matrix and state coefficient matrix can be calculated as in [13].

2.2.4   Calculating the equation of motion from A(t)
In eq. (2), the original nonlinear system model was differentiated to obtain the time-varying coefficient matrices of the linear time-periodic model, which resulted in a total derivative form for the system.

$$df = \frac{\partial f}{\partial x} dx + \frac{\partial f}{\partial u} du \tag{10}$$

In this work, only the linearized model $A(t) = \left[\partial f_i / \partial x_j \right]$ has been identified, so a model for the first term in the previous equation can be used to estimate that terms contribution to the nonlinear equations of motion. It was assumed that the coefficient matrix $\left[\partial f_i / \partial x_j \right]$ depended only on x and $\left[\partial f_i / \partial u_j \right]$ only on u. Using this assumption, the periodic orbit state vector and input components, which are known, can be used to integrate the linear time-periodic system and define the following,

$$a_{i,j}(x_j) = \int_{\bar{x}_j(t=0)}^{\bar{x}_j(t=T)} A_{(i,j)}dx_j, \quad i,j = 1,..,n, \quad n = 2N \tag{11}$$

where $a_{i,j}(x_j)$ is the integral of the component in the ith row and j^{th} column of A(t) and is taken with respect to the jth component of the state vector for all the states within the original periodic orbits. The terms in the first N rows of the $[a_{i,j}]$ matrix define the identity relationships of the state vector components, but those in the lower N rows define the force relationship of the ith degree of freedom with respect to the jth state vector component. So this method allows these dynamic forces to be individually calculated from the identified time-periodic model. The total dynamic force that acts on a degree of freedom of the system is then equal to the sum of a single row of the matrix $[a_{ij}]$, and is a function of the position and velocity states of the system.

$$a(x_d, x_v) = \sum_{j=1}^{n} a_j(x_j) \tag{12}$$

In the previous equation, a_j is the jth column of the matrix, $[a_{ij}]$. This function is directly related to the total restoring force of the system, since the following equation

$$\hat{f}(x,u) = a(x_d, x_v) + \int \frac{\partial f}{\partial u} du \tag{13}$$

Fully defines the reconstructed nonlinear equations of motion.

2.2.5 Modified Restoring Force Surface Method for Periodic Response

In this section a method is developed based on the restoring force surface approach [8] for solving for the net restoring forces over the periodic orbit from the measured periodic response. The restoring force surface method is based on the following equation of motion, which is valid for a broad range of structural systems.

$$Mx_a + g_{RF}(x_d, x_v) = F(t) \tag{14}$$

Assuming that the acceleration of each of the nodes of the system has been measured as well as the applied force $F(t)$, the restoring forces can be found as follows if one has an estimate for the mass matrix M.

$$g_{RF}(x_d, x_v) = F(t) - Mx_a \tag{15}$$

The restoring forces are functions of the displacement and velocity, and since x_a is known, x_d and x_v can be found by integrating x_a. Since x_a is the periodic response, it can be readily described by a Fourier series. As long as the constant term in the series is zero, then the Fourier series model can be integrated as in eq. (9) and then the restoring force can be plotted versus x_d and x_v or versus time over the periodic orbit.

3. Nonlinear cantilever beam system

The proposed identification method was evaluated by applying it to measurements from a nonlinear beam. Figure 1 below shows a top view photograph of the actual experimental setup. An aluminum 6061 beam is bolted to a steel mounting block, shown on the left side of the image. A small strip of spring steel is bolted to the free end of the cantilever and clamped to another steel mounting block. Both of the mounting blocks are bolted to a massive steel tube. The steel tube and mounting blocks approximate the fixed support of an ideal cantilever. The whole setup rests on a foam pad on a massive table top. The beam is oriented such that the bending axis is parallel to the plane of the table top. Figure 2 shows a close top and front view of the spring steel between the tip of the beam and the right hand side support. Table 1 below provides the physical dimensions of the beam and the spring steel in millimeters.
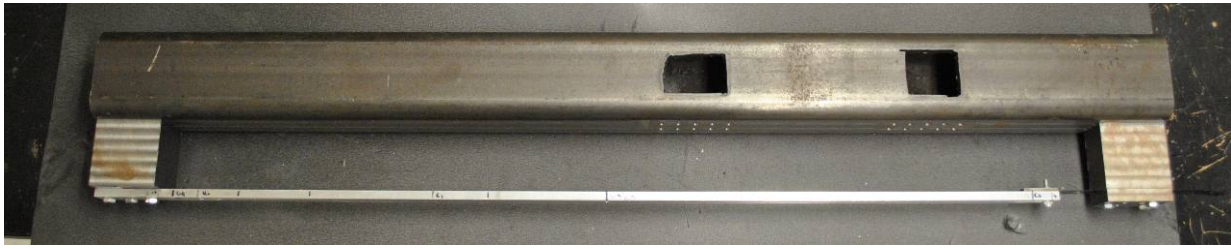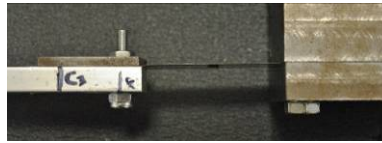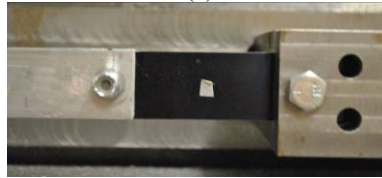
Fig. 1 Top view of the experimental nonlinear beam setup

(a)

(b)

Fig. 2 Top view (a) and front view (b) of the spring steel connected to free end of the cantilever beam

Table 1 Aluminum 6061 beam and blue-finished and polished 1095 spring steel dimensions in millimeters

Dimension	Al 6061 Beam	1095 Spring Steel
Length	1016	53.2
Width	25.4	25.4
Thickness	9.5	0.0762

The spring steel on the tip of the beam adds stiffness at that point that is geometrically nonlinear. This setup was originally proposed in [18] and other researchers have studied similar beam setups [10, 19, 20].

Figure 3 below shows a schematic of the system, which is modeled as a uniform, prismatic cantilever beam with material density ρ, elastic modulus E, cross sectional area A_b, bending area moment of inertia I, and length L. The position along the length of the beam is given by the variable 'x'. The deflection of the beam is designated with the variable y. The beam has a nonlinear tip spring with stiffness k_{nl} that is assumed to be a function of the tip displacement.
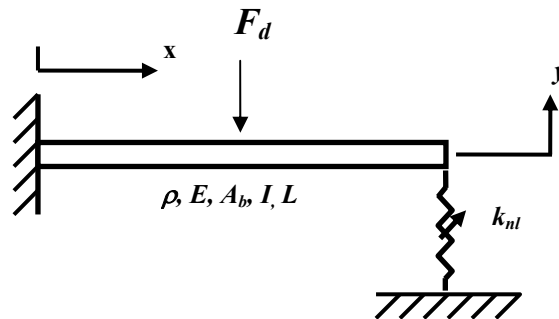

Fig. 3 Schematic of the nonlinear beam

3.1 Ritz-Galerkin Discrete Model

A Galerkin approach was used to create a finite-order model for the beam that exhibits similar properties of the experimental system. Assuming that the beam behaves linear-elastically, mode shapes corresponding to transverse bending motion were used as shape functions to construct the Ritz-Galerkin representation [21]. The displacement of the beam at a position x was approximated as

$$y(x,t) = \sum_{r=1}^{N_m} \psi_r(x) q_r(t) \tag{16}$$

where $\psi_r(x)$ is the rth Euler-Bernoulli beam mode shape for a cantilever, $q_r(t)$ is the rth generalized coordinate, and N_m is the number of modes used. The system's undamped equations of motion are provided in Eq. (17), where the coordinates are the amplitudes of the basis functions.

$$\rho A_b L [M] \ddot{q} + \frac{EI}{L^3}[K]q = Q = \sum f_{ext} \psi_r(x_f) \tag{17}$$

Modal damping was added to the equation by performing an eigenvector analysis on the linear system and then using,

$$[C] = (\rho A_b L)^2 [M][\phi_b] \big[diag(2\zeta_r \omega_r) \big][\phi_b]^T [M] \tag{18}$$

where $[\phi_b]$ is a matrix containing the eigenvectors in the columns, ω_r is the rth circular natural frequency, and ζ_r is the rth desired damping ratio. The generalized force vector Q is a sum of the product between all external forces and the value of the shape functions at the point where the force is applied, x_f. Therefore, Q includes Ritz series formulated contributions from F_d in Figure 3 as well as the restoring force due to the spring [21] The beam provides linear stiffness at the tip due to its flexural rigidity, so the spring stiffness was chosen to be purely nonlinear as given below.

$$k_{nl} = k_3 y(L)^2 \tag{19}$$

The physical restoring force due to the spring is then equal to

$$f_{sp} = k_3 y(L)^3 . \tag{20}$$

The generalized force vector then has components corresponding to the nonlinear spring $\{Q_{sp}\}$ located at $x=L$ and the externally applied force $\{Q_{ext}\}$ located at $x=x_f$.

$$\{Q\} = \{Q_{sp}\} + \{Q_{ext}\} = k_3 y(L)^3 \begin{Bmatrix} \psi_1(L) \\ \vdots \\ \psi_N(L) \end{Bmatrix} + F_D \begin{Bmatrix} \psi_1(x_f) \\ \vdots \\ \psi_N(x_f) \end{Bmatrix} \tag{21}$$

The external force is given by the following.

$$F_D(t) = A\sin(2\pi f t) + A_{impulse} \sin\left(\frac{\pi}{\tau}(t - t_p)\right) \tag{22}$$

where A is the amplitude and f is the frequency of the periodic forcing term, and $A_{impulse}$ is the amplitude of the impulsive forcing term, which is used to perturb the system from the periodic orbit. The impulsive force has duration $\bar{\tau}$ and is initiated at t_p.

After using the Ritz-Galerkin method to form the discrete beam model and to account for the nonlinear applied force of the spring, the equations of motion were transformed back into physical coordinates using the relationship in eq. (16). The differential equations of motion can then be arranged in state space format.

$$\begin{Bmatrix} \{\dot{y}\} \\ \{\ddot{y}\} \end{Bmatrix} = \begin{Bmatrix} \{\dot{y}\} \\ -[M_p]^{-1}\big([C_p]\dot{y} + [K_p]y + \{F\}\big) \end{Bmatrix}$$

$$[M_p] = \rho A_b L [\Psi]^{-T}[M][\Psi]^{-1}, \quad [C_p] = [\Psi]^{-T}[C][\Psi]^{-1}, \tag{23}$$

$$[K_p] = \frac{EI}{L^3}[\Psi]^{-T}[K][\Psi]^{-1}, \quad \{F\} = [\Psi]^{-T}\{Q\}$$

The matrix $[\Psi]$ has the numerical values of the mode vectors for specific position coordinates on the beam. Since this matrix must be square in order to form an inverse, it is convenient to choose the number of degrees of freedom in the system to be equal to the number of modes used in the Galerkin expansion. Then, $[\Psi]$ can contain shape functions evaluated at the nodal degrees of freedom on the beam. In this study the number of mode shapes used in the expansion and the number of degrees of freedom used to model the beam was $N_m=N=2$. The degrees of freedom were located at the center and tip of the beam.

In order to mimic the experimental system, the following parameters were used in the model, which are based on the nominal properties of the experimental hardware: ρ=2700 kg/m^3, E=68e9 N/m^2, A_b=3.23e-4 m^2, I = 4.34e-9 m^4, L = 1.016 m. Using these properties with the Ritz-Galerkin method, the two linear natural frequencies of the system are $\omega_1/(2\pi)$= 9.97 Hz and $\omega_2/(2\pi)$=62.51 Hz. The transverse stiffness contribution of the spring steel on the experimental beam is approximated in the model as k_3=1.4764e9 N/m^3. A derivation of this approximation can be found in the appendix.

3.2 Simulated Measurements

In order to apply the proposed nonlinear identification, the nonlinear beam must first be driven to respond in a periodic orbit. However, there are many possible periodic orbits that this system may be driven in so it is desirable to consider all of the possible periodic orbits for different forcing configurations. In a companion paper [22], the authors used a numerical continuation technique to calculate the periodic solutions of the beam model for forcing amplitude of A=1 Newton and for forcing frequencies in the band 6-70 Hz. The results of the computation are shown in Figure 4. In (a) and (b), the response curve near the first linear natural frequency is plotted. The red and blue curves in (a) correspond to the displacement initial conditions of the first and second degree of freedom, respectively. The green and black curves in (b) are the analogous velocity initial conditions. This color format is repeated in (c) and (d) for the frequency band near the second linear natural frequency. The curves quantify the resonant responses of the first and second modes of the nonlinear beam (referenced to zero phase of the force), but they also provide the initial state vector for a specific frequency that one can integrate in time to achieve a periodic orbit. A detailed discussion of the dynamics of the frequency response curves is provided in [22]. The important implications of these nonlinear frequency response curves is that the resonance peaks tend to bend towards higher frequencies for this system, which causes regions where multiple periodic orbits are possible for a single forcing frequency, and for this system one of those possible solutions is unstable (unstable solutions are designated in the plots with the dashed lines). The forcing configuration needs to be carefully selected in order to achieve a successful identification of the nonlinear parameters. Guidelines for selecting forcing configurations for the system identification method used here are discussed in detail in [14] for a single degree of freedom system, and those guidelines apply equally well here.
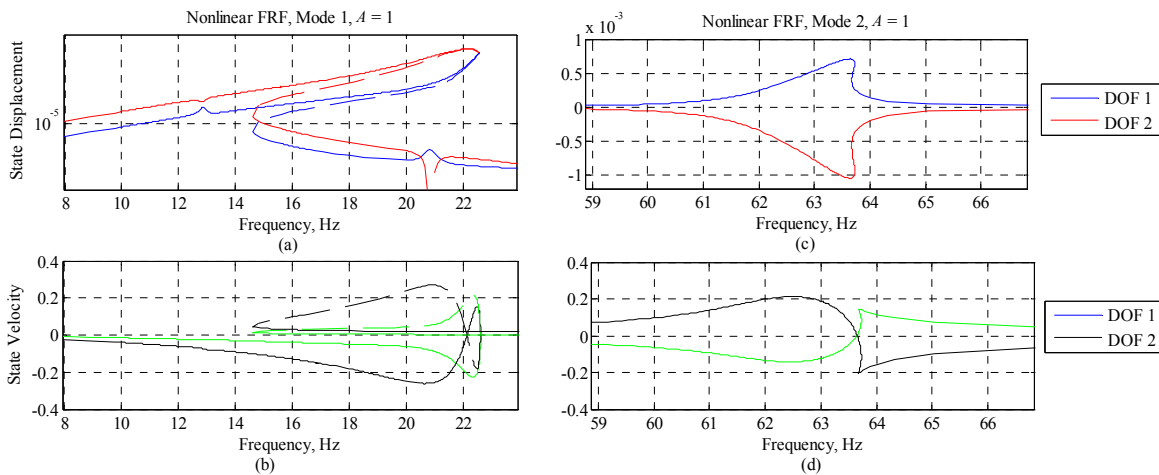

Fig. 4 Initial conditions that result in periodic responses for A=1 plotted versus forcing frequency

The nonlinear frequency response curves were used to understand what types of periodic orbits were possible, and a few of the different alternatives were selected for study. It is desirable to drive the system in a stable periodic orbit that is sufficiently nonlinear and isolated from other nearby stable periodic orbits. Sracic and Allen [14] showed that periodic orbits on the larger amplitude branch of the bent resonance peak tend to provide suitable periodic orbit conditions to use for the identification procedure for a hardening resonance such as that of the peak in Figure 4(a). Therefore, a forcing frequency of f_1=15.4 Hz was chosen on the first resonance peak of Figure 4(a). Since the beam model has two modes that produce resonance responses, a second forcing frequency of f_3=60.9 Hz, which is just below the second resonance peak of Figure 4(c),

was chosen to explore the results of the identification when the periodic orbits from different modes are used. For each case, the procedure that was employed in [14] is also used here to simulate the response and perform the identification. First, the acceleration periodic and periodic plus perturbation responses are simulated using MATLAB's 4-5th order Runge-Kutta integrator function 'ode45'. (Although the discrete system is derived for a state vector consisting of all the displacement and velocity states, 'ode45' allows one to extract the acceleration states of the system from the calculation as well.) For each response, the amplitude of the harmonic forcing was A=1 N and the amplitude, duration, and time of initiation of the impulsive force were $A_{impulse}$=10 N, $\bar{\tau}$ = 0.02 seconds, and t_p=0 seconds (the impulsive force was set to zero when computing the periodic response). The response was calculated for a time history that was long enough for the perturbation to decay such that only the underlying periodic orbit response remained.

Case 1:
The responses were calculated from initial conditions $[y\ \dot{y}]$=[-3.517e-5; -1.223e-4; 3.639e-2; 0.1160], which define the periodic orbit at 15.4 Hz relative to zero phase on the forcing function, and the solution was sampled at a 616.4 Hz, which gave 40 samples per period of the periodic orbit. Figure **5** shows the time history of the tip degree of freedom both early (a) and late (b) in the response. The periodic response is plotted with the dashed blue curve and the periodic plus perturbed response is plotted with the solid red line. The difference between the periodic and perturbation responses is plotted in (c) with the solid black line, and this plot shows that the perturbation is small compared to the periodic response and that it eventually decays to approximately zero, meaning the response has returned to the periodic orbit. The responses of the beam midpoint degree of freedom are not shown, but they were in phase with the tip responses shown here and have similar characteristics but smaller extreme amplitudes.
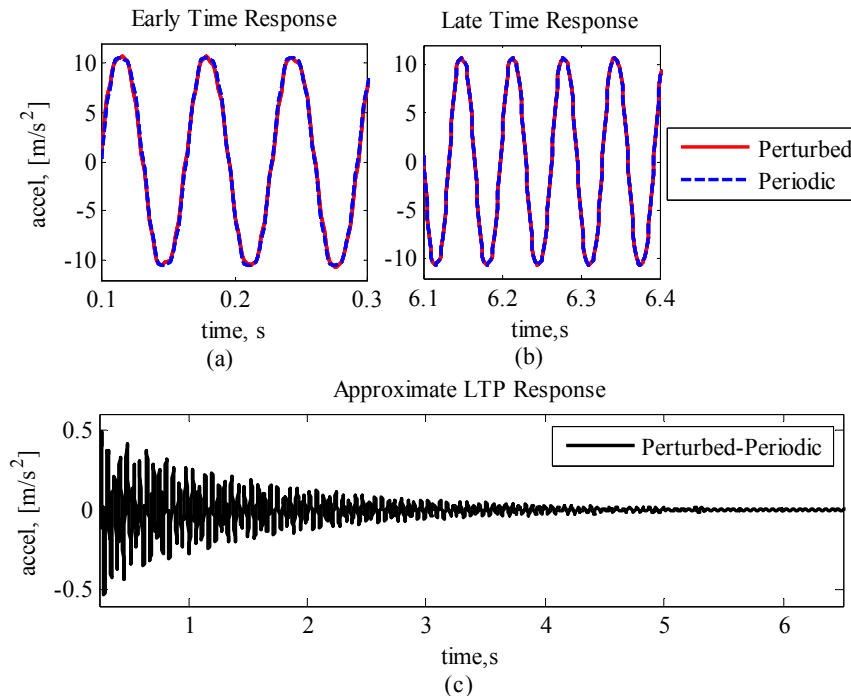

Fig. 5 Tip responses of the beam model for forcing frequency f_1=15.4 Hz

The spectra of the perturbed responses and those of the difference between the perturbed and the periodic response were calculated with the Fast Fourier Transform (FFT) algorithm in MATLAB and are plotted in Figure 6(a) and (b) for the midspan and tip degrees of freedom, respectively. The perturbed responses are plotted with the solid red lines and the perturbed minus the periodic responses are plotted with the dashed black curves. The red curves contain a number of sharp peaks at the frequencies 15.4, 46.2, 77, 107.8, and 138.6, and the magnitudes of these peaks diminish with increasing frequency. These frequencies correspond to the forcing frequency and a few of its odd harmonics (e.g. 3*15.4 Hz = 46.2 Hz). The spectra of the red and black curves also contain a number of broad peaks near 12.6, 18.2, 43.4, 49, 65.8, 74.2, 79.8, 96.6, 110.6, and 127.4 Hz in both degrees of freedom, at 35 Hz in the first degree of freedom, and at 105 Hz in the second degree of freedom.
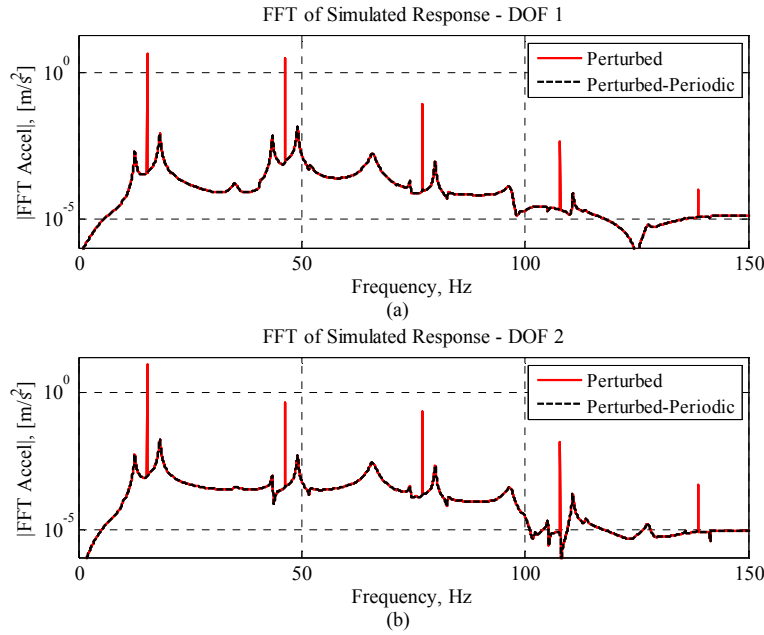
Fig. 6 Response spectra of the nonlinear beam simulation for forcing frequency f_1=15.4 Hz

The response of the beam is strongly nonlinear, since a single harmonic input was applied at 15.4 Hz, and the system responded at that frequency as well as at a number of its harmonics. The broad peaks in the response all seem to have the characteristics of linear mode peaks; Eqs. (5) and (8) can be used to understand that many of these peaks are due to time-periodic effects of the perturbation about the periodic orbit. For example, the peaks at 12.6 and 18.2 Hz have similar characteristics to the peaks at 43.4 and 49, and the two peak clusters are separated by 30.8 Hz, which is twice the fundamental frequency of the periodic orbit. These two peak cluster seems to be repeated at intervals of 30.8 Hz, although the magnitudes of the peaks change. The peaks at 35, 65.8, and 96.6, and 127.4 Hz are also increasing in frequency by 30.8 Hz and have similar characteristics albeit different magnitudes. The fact that many of these peaks seem to be related and occur at frequencies that can be linked by the fundamental periodic orbit frequency is strong evidence that the system is behaving time-periodically about the orbit. Noise or some other artifact in the response is not likely to have the characteristic shape of a mode nor to occur at frequencies that are related by the periodic orbit frequency.

In order to fit a time-periodic model to the perturbed minus the periodic responses, the lifting technique [13] was used to resample the responses into a set of 'lifted responses' that are exemplary of the responses exhibited by a lower-order linear time-invariant system. The composite spectra (or average) of the lifted responses is plotted in Figure **7** with the solid black line, and it contains one prominent peak near 2.8 Hz and a much weaker, broader peak near 4.2 Hz. The Algorithm of Mode Isolation (AMI) [23] identified two modes in the composite response spectra. A reconstruction of the two mode fit is plotted in the figure with the dashed line. The difference between the response curve and the fit is plotted with the dashed-dot gray curve, and it shows that the two-mode fit approximates the response very well. AMI identified two eigenvalues λ_1= -0.7310 +17.6158i and λ_2= -3.9901 +26.2590i, natural frequencies $|\lambda_1|/(2\pi)$=2.806 Hz and $|\lambda_2|/(2\pi)$=4.227 Hz, and damping ratios 0.0415 and 0.1502, respectively.
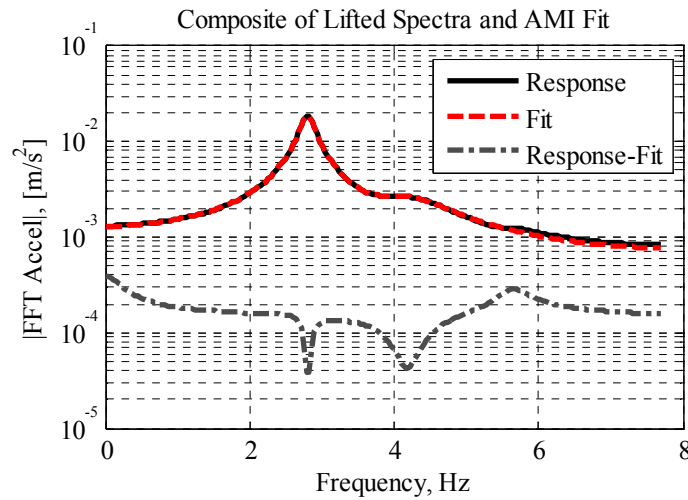
Fig. 7 Composite spectrum and AMI fit of the lifted responses forr forcing frequency f_1=15.4 Hz

The lifting technique is advantageous because any peaks in a response that are due to time-periodic mode effects are collected to a single peak, so the underlying order of the system is more easily determined; even though the spectra in Figure 6 contain many peaks, the composite spectrum of the lifted responses shows clearly that the system has only two dominant modes. The modal fit obtained by AMI provides the time-periodic mode shapes of the system for one full period of the underlying periodic orbit. The next step towards constructing the state transition matrix and state coefficient matrix of the linear time-periodic system is to expand the identified mode shapes in a Fourier series and to determine which Fourier coefficients contribute meaningful information to the response. This process is clearer if the identified time periodic modes are first unaliased (a discussion of aliasing due to lifting can be found in [13, 24]).

After the identified modes were unaliased, they were expanded in a Fourier series. Figure 8 shows a plot of the amplitudes of each of the coefficients in the Fourier series expansion of Mode 1 (a) and Mode 2 (b). The open blue circles designate all of the coefficients calculated in the expansion. The red dots designate the Fourier coefficients that will be retained in the linear time-periodic model when computing $A(t)$.
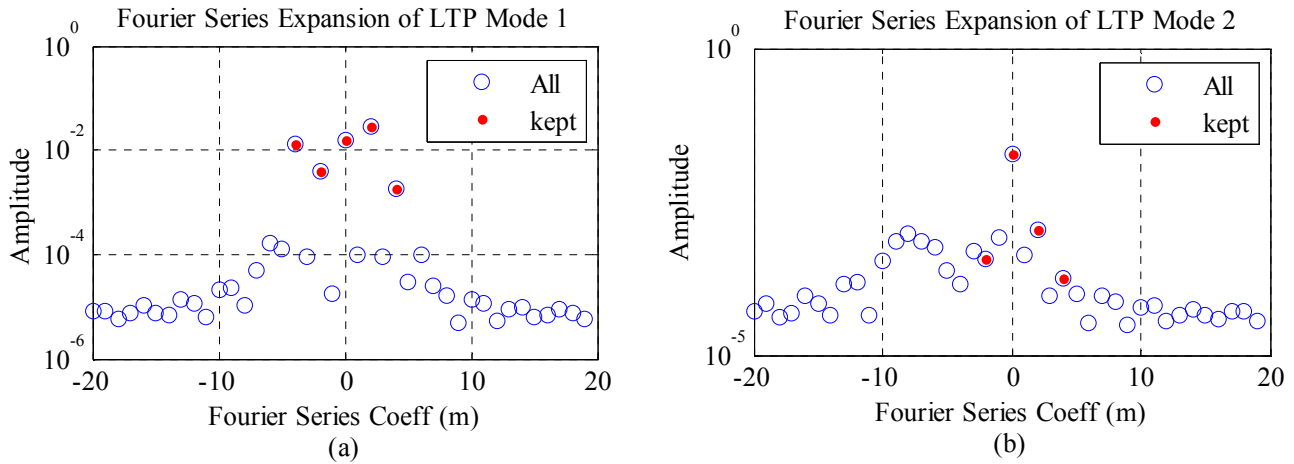

Fig. 8 Fourier series expansions of the identified modes for forcing frequency f_1=15.4 Hz

For the first mode, the dominant coefficients were easily determined because of their large amplitude relative to the others. One can verify that these coefficients are important to the response by interrogating the spectra in Figure 6(a) and (b) for the corresponding peaks. It was determined that the unaliased Floquet exponent was attributed to the peak at 18.2 Hz, so this is the m=0 harmonic in the Fourier series expansion. The peaks at 49, 79.8, and 110.6 Hz can be attributed to the m = +2, +4, and +6 harmonics (i.e. 18.2+2*15.4= 49, 18.2+4*15.4 = 79.8, and etc.). The peaks at 12.6, 43.4, 74.2, 105 Hz can be attributed to the m=-2, -4, and -6 harmonics since for example, 18.2-2*15.4= -12.6 and negative frequencies reflect back to positive frequencies. The Fourier series expansion in Figure 8 reveals that the harmonics m=-4,-2,0,+2,and +4, have larger amplitude than the baseline noise, so only those are retained when forming $A(t)$.

The dominant coefficients of the second mode (b) are more ambiguous. One might presume from Figure 8(b) that only the $m=0$ term is significant. However, the spectra from Figure 6(a) and (b) show that there are significant time-periodic peaks at 35, 96.6, and 127.4 Hz that can be resolved from the noise. Since the Floquet exponent of this mode is 65.8 Hz, these peaks correspond to the $m=-2$, $+2$, and $+4$ harmonics of the expansion, and because the peaks in the spectra can be resolved from noise they are physically meaningful and should be retained in the Fourier series expansion of the mode.

After the Fourier series models of the identified modes have been formed, they were integrated twice according to Eq. (9) in order to obtain a description of the modes in terms of displacement. Then, the state transition matrix and state coefficient matrix were constructed based on the method in [13]. An analytical model for the state coefficient matrix was also constructed using the same method as in [14]. The system is fourth order, so the state coefficient matrix is a 4x4 time dependent matrix. The lower left 2x2 block corresponds to scaled stiffness components of the model. The (3, 2) and (4, 2) components of the state coefficient matrix, which are the stiffness coefficients that multiply the beam tip degree of freedom are plotted versus time in Figure 9. The components that were estimated using the proposed identification method are plotted with open circles, and the analytical coefficient values are plotted with a solid line. The analytical (3, 2) component of the matrix (black line) varies over the periodic orbit by approximately 30% of its initial value of 3.46e4 [N/(kg-m)], and the analytical (4, 2) component varies by approximately 51% of its initial value of -5.26e-4 [N/(kg-m)], so the system is quite time periodic based on the analytical model. The estimated coefficients for the (3, 2) and (4, 2) terms of the state coefficient matrix agree fairly well with the analytical values. The (3, 2) term differs from the analytical term by at most about 8.5% and the (4, 2) term differs by at most about 12.5%.
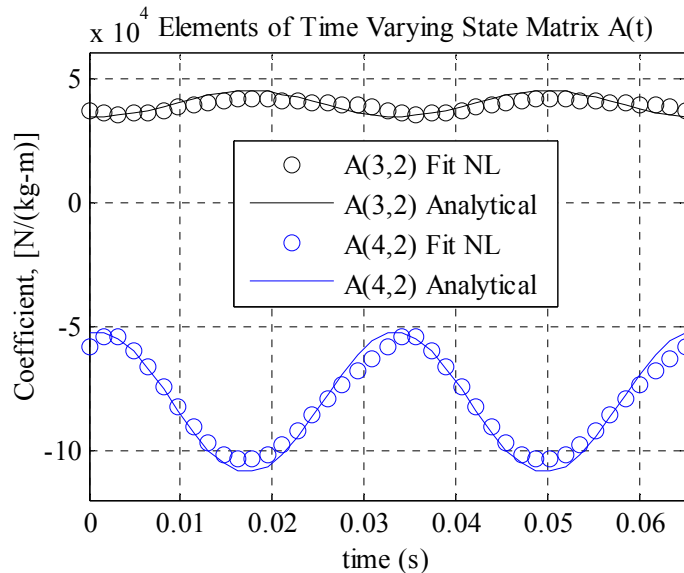

Fig. 9 Time-periodic state coefficient matrix components for forcing frequency f_1=15.4 Hz

The (3, 1) and (4, 1) terms of the state coefficient matrix are also related to the stiffness of the system, but for brevity they are not shown. The analytical (3, 1) and (4, 1) terms are constant, but their estimates showed between 8% and 14% variation with time, although they were relatively accurate in an average sense.

Because the damping in the system is linear, the lower right 2x2 block of the true analytical state coefficient matrix is also composed of terms that are constant with time. The estimates of these damping terms from the identification method vary significantly with time. Each of the four terms varies by an amount that is at least an order of magnitude larger than the constant value predicted by the analytical model, and they did not tend to agree very well in an average sense either. However, the identified STM matched the decay of the actual response well, so the error seems to arise when estimating $A(t)$ from the STM.

The identified state coefficient matrix can now be used to calculate its force contributions to the equations of motion of the nonlinear system according to eq. (11). This was done using MATLAB's 'cumtrapz' function, which is an approximation of the cumulative integral using the trapezoidal method. The lower left-2x2 block of the matrix in eq. (11) is plotted in Figure 10 versus the corresponding displacement term. Since these terms were integrated with respect to the displacement components of the state vector, they are the scaled force-displacement functions of the system. The top row of plots relates

to the first degree of freedom (DOF) and the bottom row the second DOF. The identified scaled force-displacement curves are plotted with the open blue circles. The analytical state coefficient matrix was also integrated according to eq. (11). The scaled force-displacement curves for the analytical system are plotted with the blue lines. The underlying periodic orbit defines the displacement of the DOFs, and the first DOF displaces between about ±0.5mm ((a) and (c)), while the second DOF displaces farther, between about ±1.2mm ((b) and (d)). The restoring force on the first DOF ($a_{1,1}$) has a negative correlation with y_1 displacement. This is also seen for the $a_{2,2}$ versus y_2 relationship, while both the cross terms ($a_{1,2}$ and $a_{2,1}$) are positively correlated. The magnitudes of the [$a_{1,1}, a_{1,2}$] and [$a_{2,1}, a_{2,2}$] force components oscillate between about ±50 N/kg and ±90 N/kg, respectively. All the force-displacement curves are predominantly linear, except for the $a_{2,2}$ component in (d). The identified force-displacement relationships agree exceptionally well with the analytical relationships.
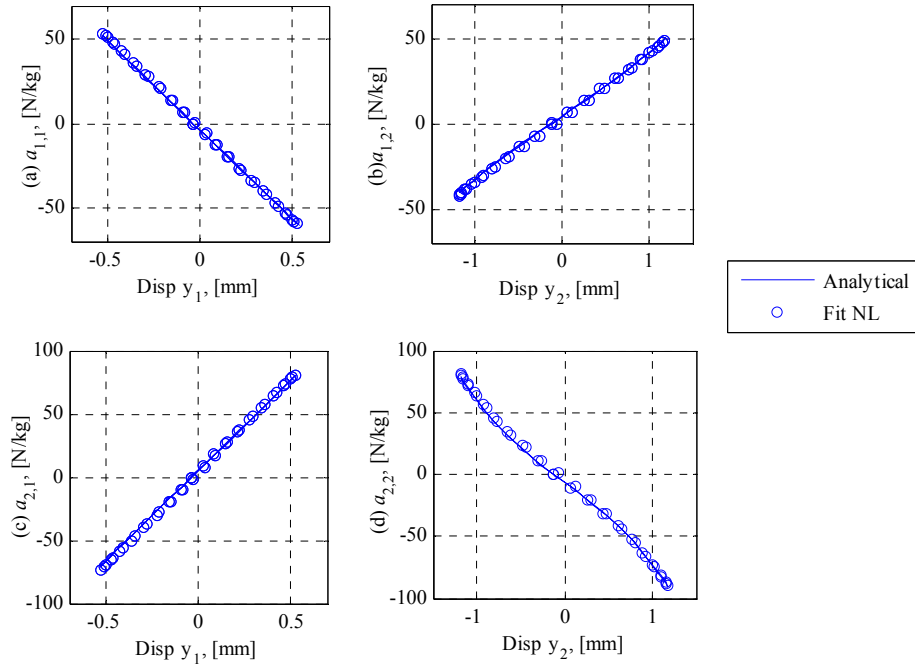

Fig. 10 Scaled force-displacement relationships acting on the beam DOFs for forcing frequency f_1=15.4 Hz

The forced-displacement curves can be directly linked to the dynamics of the system and how the DOFs interact. These functions completely characterize the nonlinear equation of motion of the system. According to these results, only the beam tip is subjected to nonlinearity, and this is consistent with the location of the nonlinear spring. It is significant that these results were obtained without any a priori assumption regarding the shape of the force-displacement relationships.

The force displacement relationships that have been identified for the system can be validated to some degree by using them to compute the total restoring force in the system at each point within the periodic limit cycle. This sum of the restoring forces can also be computed using the method described in Section 2.2.5, and the two can be compared to validate the results. To do this, each block of terms must be premultiplied by the analytical mass matrix to achieve the same scaling. This puts the terms into units of force rather than units of acceleration. The restoring forces have components due to the stiffness of the beam and due to the dissipative effects of damping. The total restoring force acting on a degree of freedom is the sum of these, but it has already been noted that the damping estimates are questionable, so the restoring forces were computed both with and without the damping terms. Figure 10 shows the restoring forces versus time for one cycle of the periodic orbit. The total restoring force estimate (RF$_{LTP}$ Total) is plotted with the open blue circles. The estimate that excludes the velocity related forces is labeled (RF$_{LTP}$ Disp.) and plotted with open black squares. The total restoring forces computed using the RFS method outlined in Section 2.2.5 are also shown with the solid blue line. In the first half of the orbit, the restoring force on the beam tip leads the restoring force on the beam center, which initially remains near zero, but both forces are in phase and increase to a maximum near 0.017 seconds. The maximum value of the analytical restoring force is near 5 N for the beam center and 2 Newton for the beam tip. After the maximum, both restoring forces decrease towards zero, and the force on the beam center reaches the near zero around 0.03 seconds, while the force of the beam tip goes through zero near the half period time of 0.033 seconds. The restoring forces during the second half of the period are antisymmetric to the first half. In

general, the estimated total restoring force that acts on the beam center agrees very well with the force computed using the RFS method. However the estimate at the beam tip shows significant discrepancies when the damping terms are included. This reveals that the damping in the linear time-periodic model has not been accurately identified, but the actual damping is small so we can verify that the displacement dependent terms have been properly identified.
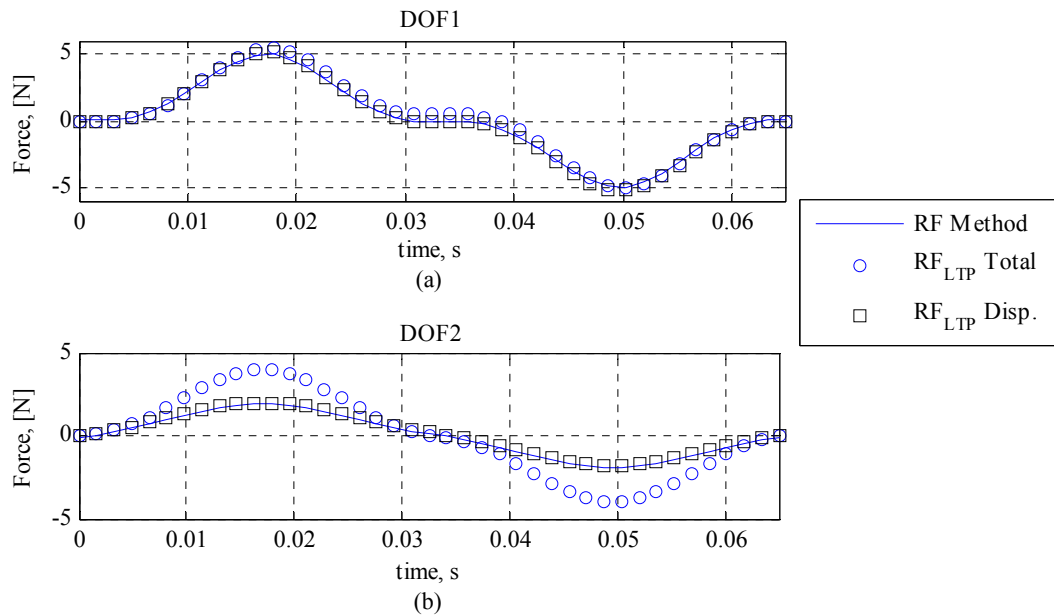

Fig. 11 Time-periodic restoring forces acting on the beam degrees of freedom for forcing frequency f_1=15.4 Hz

Discussion

Using the proposed identification method, a functional form of the force-displacement and force-velocity (not shown) relationships was directly calculated. Each term of the state coefficient matrix that was directly related to a parameter of the system was integrated individually to produce a force relationship. This approach also allows one to separate the effects of stiffness and damping, thereby using only the trustworthy identified parameters. For example, the components of the estimated state coefficient matrix that related to damping contained a measurable amount of error, so those terms could be approximated with some other method to achieve a more trustworthy model. Additionally, this method allows one to evaluate how errors in each identified state coefficient component are transferred to the force relationships. Even though the estimated (4,2) term of $A(t)$ was different than the analytical term by up to 12.5%, the estimated $a_{2,2}$ force-displacement curve compares remarkable well to the analytical model. Finally, the method provides important information on the interaction of the multiple-degrees of freedom. The $a_{2,2}$ curve provided evidence that DOF y_2 was subjected nonlinear effects, and it could be used to extract the functional form of the nonlinearity.

Case 2:

The system may also be driven in a periodic orbit near the second resonance condition, which will also produce a large amplitude response that maps a large portion of the state space. In order to assess the results of the identification when using different resonance conditions, a second simulation case was considered with forcing at f_2=60.9 Hz. The system was simulated from initial conditions $[y \; \dot{y}]$=[-8.631e-5; 1.217e-4; 9.103e-2; -1.345e-1], and the same procedure as Case 1 was used to calculated the periodic and perturbed responses for the same harmonic forcing amplitude and impulsive forcing configuration. The time histories in this case were similar to those shown for the previous case, only now the two measurement points are out of phase since the second mode dominates the response.

The spectra of the perturbed responses and those of the difference between the perturbed and the periodic response responses were calculated with the FFT function, and those curves are plotted in Figure 12(a) and (b). The periodic response at the drive frequency 60.9 Hz and at the third harmonic of the drive frequency, 187.2 Hz, are both clearly visible, as well as several peaks due to the time-periodic effects caused by the nonlinearity. The lifting technique was applied as before, and the

composite spectrum of the lifted responses is plotted in Figure 12(c) with the solid black line. The lifting technique again results in a much simpler spectrum, and there are two prominent peaks at 1.85 Hz and 11.6 Hz and a very weak peak at 23.2 Hz in the composite of the lifted responses. There also seems to be some high amplitude response near the zero frequency line. AMI identified two modes in the responses with eigenvalues λ_1= -3.9850 +11.5712i and λ_2= -0.6290 +72.8480i, natural frequencies $|\lambda_1|/(2\pi)$= 1.9478 Hz and $|\lambda_2|/(2\pi)$=11.5945 Hz, and damping ratios 0.3256 and 0.0086, respectively, and a composite of the reconstruction of the responses from the two mode fit is plotted with the dashed red curve. The subtraction residual is substantially reduced by the two mode fit, but some artifacts remain near the zero frequency line and near 23.1 Hz.
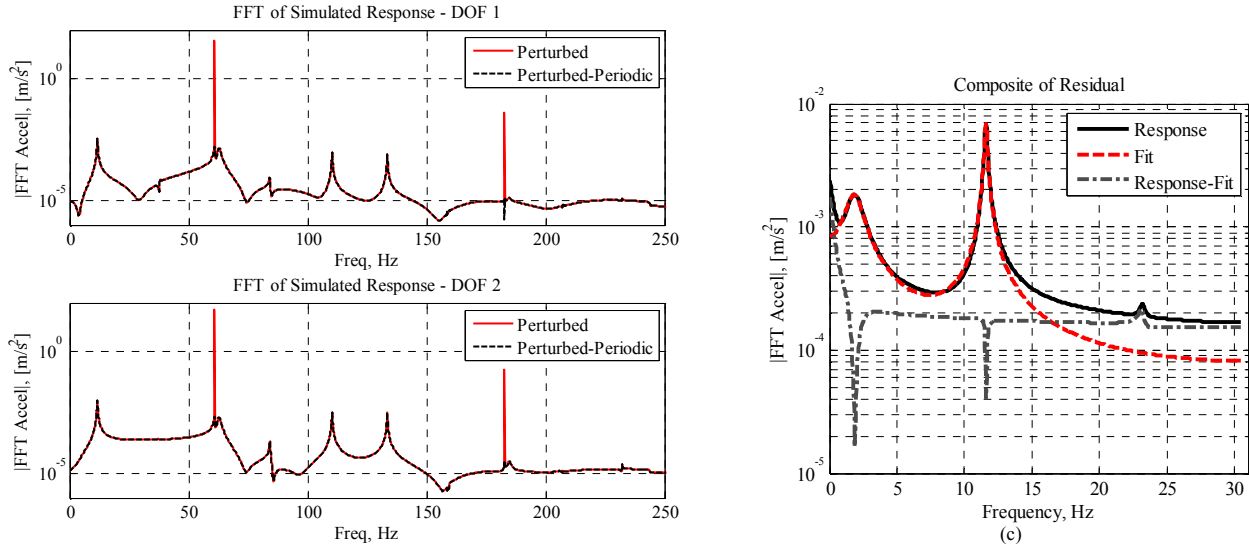

Fig. 12 Response spectra for forcing frequency f_2=60.9 Hz

The spectra from the perturbed response contain far fewer peaks than with the Case 1 forcing. The peak near 11.6 Hz in (a) and (b) directly corresponds to the 11.6 Hz peak in the composite of the lifted responses, so AMI identified an unaliased eigenvalue for this mode in this case. The peaks at 110.2 and 133.4 Hz in (a) and (b) can be attributed to the m=-2 and +2 harmonics of the time periodic mode at 11.6 Hz, since 11.6-2*60.9 Hz = -110.2 Hz, which reflects back to a positive value, and 11.6+2*60.9 Hz = 133.4 Hz. The broad peak at 62.8 Hz becomes aliased in the composite spectrum of the lifted responses and corresponds to the peak at 1.85 Hz in (c). This eigenvalue can be unaliased by adding 2π*60.9 rad/s to the imaginary part of the eigenvalue for this peak, which results in the natural frequency $|$-3.985 +394.4i $|/(2\pi)$ = 62.77 Hz that matches the peak in (a) and (b). The other notable peaks at 37.8 Hz in (b) and 84 Hz in (a) and (b) cannot be attributed to time-periodic effects of the identified modes. These peaks differ from the drive frequency by -23.1 Hz and +23.1 Hz for the 37.8 and 84 Hz peaks, respectively, so they both alias to 23.1 Hz in the composite of the lifted responses. Those peaks may be [14] caused by the domain of attraction [25] of a nearby (in state space), strong, and stable periodic orbit (e.g. the perturbation about the limit cycle may not be sufficiently small). The cause of such artifacts and their quantitative effect on the identification results will be a focus of future works.

The responses for this forcing case contain fewer time periodic effects than in the previous case, and thus the Fourier series expansion models of the mode shapes are quite straightforward to construct. The Fourier series were formed for each mode shape, and the m=-2, 0, and +2 terms were retained for the 11.6 Hz mode (λ_2 from AMI) and only the m=0 term was retained for the 62.8 Hz mode (λ_1 from AMI before unaliasing). Then, the Fourier series expansions of the modes were integrated twice to get displacement models and used to construct the state transition matrix and state coefficient matrix of the time-periodic model. The estimated values of the (3, 2) and (4, 2) terms of the identified state coefficient matrix are plotted in Figure 13 with the open circles. The analytical state coefficient model was also calculated for this forcing case, and the values of the analytical coefficients are plotted with solid lines. The analytical (3, 2) coefficient varies throughout the period by about 3% of its minimum magnitude, and the analytical (4, 2) coefficient varies by about 11%, so this model is not as strongly time-periodic as the model from forcing Case 1. The terms from the estimated state coefficient matrix agree well with the analytical model, differing by about 2% and 7% over the course of the periodic orbit, respectively. The (3, 1) and (4, 1) terms from the estimated state coefficient matrix vary by relatively small amounts over the course of the period, but their mean values over time agree very well with the constant analytical values for those matrix terms. Like forcing Case 1, the estimates for the state coefficient terms that are related to damping (in the lower right 2x2 block) tend to vary over the course of the period with large errors. However, fluctuations in these terms are not as large as those of forcing Case 1.
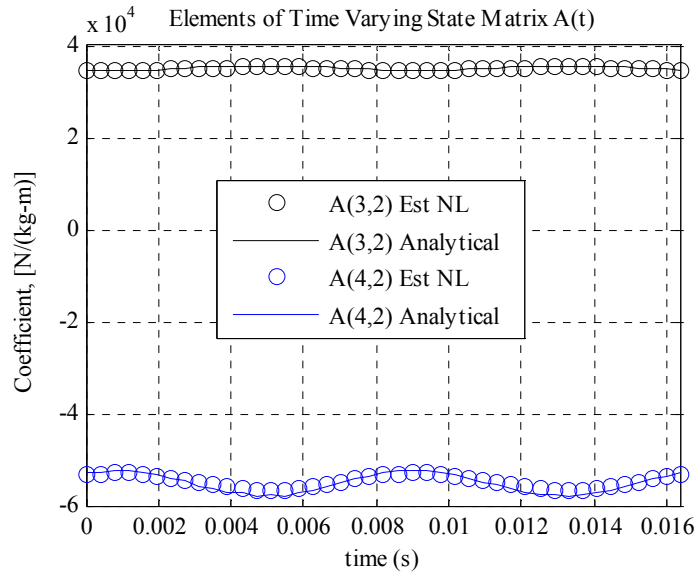
Fig. 13 Time-periodic state coefficient matrix components for forcing frequency f_2=60.9 Hz

The estimated state coefficient matrix was used to calculate the restoring forces using the same method as for forcing Case 1. The left-2x2 block of the resulting function g is plotted in Fig. 14 for the estimated and analytical force-displacement relationships using open black squares and solid black lines, respectively. The force-displacement results from the Case 1 identification are also shown with open blue circles and solid blue lines for the estimated and analytical results. The displacements of the DOFs for this periodic orbit are much smaller than the previous case, and correspondingly the magnitudes of the restoring forces are also smaller. The force-displacement curves for Case 2 have the same correlation with the DOFs as Case 1, with the diagonal terms that are plotted correlated negatively and the off diagonal terms correlated positively. Although the Case 2 estimated force-displacement values agree very well with the Case 2 analytical values, there appears to be some offset between curves from Case 1 and Case 2. However, the slopes of the curves between the displacements that are shared for both cases agree very well
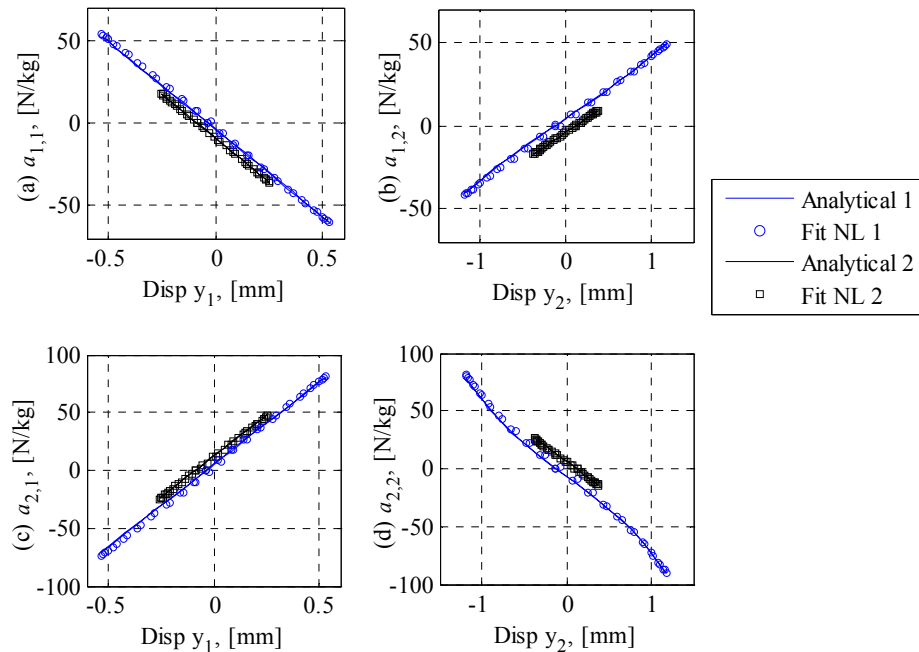

Fig. 14 Time-periodic restoring forces acting on the beam degrees of freedom for forcing frequency f_2=60.9 Hz (the Case 1 results are shown for comparison)

Discussion

When the system was excited with a frequency near the second nonlinear resonance, a very different periodic orbit was produced. The DOF responses were out of phase, and the magnitudes of the displacements were smaller. Despite the differences of the periodic orbit and interaction of the DOF, the procedure was still very straightforward to apply, and a trustworthy time-periodic model was identified. Due to the smaller amplitudes of the DOFs, the model contained less time-periodic effects, and the force-displacement relationships that were constructed were only weakly nonlinear. Nevertheless, these curves did match the linear slope of the Case 1 force displacement model providing good evidence that the two models are in agreement. It is clear from the results that the Case 1 forcing configuration provides better opportunity to identify a nonlinear model of the system. The higher frequency can be used, but the system must then be forced at higher amplitude in order to better excite the nonlinearity.

3.3   Experimental Measurements

The identification method was next applied to the experimental system. Harmonic excitation was applied to the beam with a model 2100E11-100 lb Modal Shaker from The Modal Shop, Inc. The beam was approximated as a having a fixed support, so the shaker was freely hung from a lateral excitation stand, as recommended in [26] for shaker excitation. A thin steel stinger was used to transmit the excitation from the shaker to the beam. One end of the stinger was clamped inside the shaker armature and the other end was fixed to a force transducer, model 208C04 from PCB Piezotronics, Inc. (PCB), which was bolted to the beam at a location x = 508 mm from the fixed end of the beam. Harmonic forcing was provided by a Textronix model 3022 arbitrary function generator, amplified by a model 2050E05 power amplifier from The Modal Shop, Inc., and input to the modal shaker. The amplitude and frequency of the excitation were varied to find forcing conditions that drove the beam to respond in a desirable stable periodic orbit. A modally tuned impulse hammer, model 086C01 from PCB was used to impact the beam at various locations to disturb the response from its periodic orbit. The response was measured with an Endevco model 66A12 triaxial accelerometer (z-channel was used) located at x = 508 mm (beam center) and with an Edevco model 256-100 isotron accelerometer located near the free end of the beam at x = 984mm (beam tip). All the accelerometers were secured to the beam with wax. The measurements were acquired using a Photon II portable dynamic signal analyzer by LDS Dactron. This system was also used to apply sine-sweep forcing signals.

An initial sine sweep test was performed to evaluate the frequency response of the beam from 1-150 Hz. The Photon II output voltage was set to 0.2 Volts for this test (the gain on the amplifier was held at a constant level for all tests). The frequency was swept from 1-150Hz in a period of 699 seconds, and the acceleration responses of the beam and the applied force response were measured during this sweep. The Hilbert Transform was applied to these signals to determine the instantaneous amplitude and frequency for all time instants during the sweep. Then, a moving average with a ten sample bandwidth was applied to the results of the transformed signals and the ratio of the response to the force was calculated at each frequency line. Figure 15 shows the nonlinear frequency response computed in this way, with the beam center degree of freedom plotted with the blue curve and the beam tip plotted with the red curve. There are a number of peaks in the spectra below 150 Hz, including two broad peaks near 17 and 43 Hz, two very weak peaks near 30 and 60 Hz, and a prominent sharp peak near 120 Hz. Both of the broad peaks are very noisy despite the smoothing that was applied to the signals. The lowest frequency peak in particular is very irregular below 17 Hz in both degrees of freedom. Near 37 Hz, there appears to be a large discrete jump in the amplitude of degree of freedom one and a small jump in the amplitude of the tip.
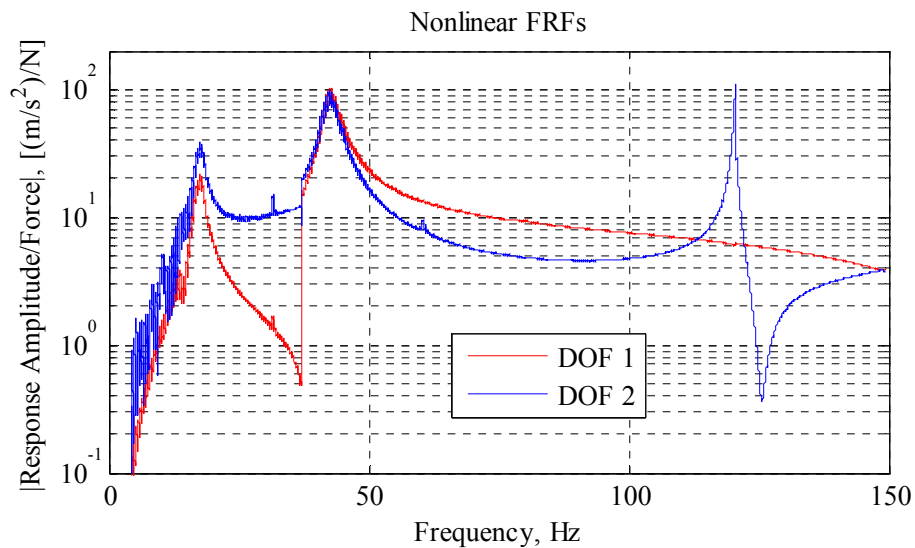
Fig. 15 Nonlinear frequency response of the experimental nonlinear beam for DOF 1(midspan) and DOF 2(tip)

The peaks in the nonlinear frequency response can be deciphered using knowledge of the underlying linear system. The third linear bending mode of a cantilever will tend to have significant tip response but minimal beam center response (due to a nearby node), so the peak near 120 Hz could be related to the third linear bending mode and appears to be predominantly linear. The peaks at 17 and 43 Hz could then be related to the first and second linear bending modes, respectively. All the remaining artifacts in the responses must be attributed either to noise or the nonlinearity of the system. The jump in the amplitude of the responses is a typical characteristic of nonlinear systems, so it can be assumed that the system responds nonlinearly when forced near these frequencies. The jaggedness of the curve below 17 Hz seems to be caused both by super harmonic resonances in that region and by limitations of the shaker and setup at these low frequencies. Therefore, a forcing frequency of 20 Hz was selected to drive the system and apply the proposed identification, since it is near the 17 Hz peak and both degrees of freedom are adequately excited at this frequency.

The function generator was used to drive the system at 20 Hz with amplitude of 0.2 Volts. The impact hammer was used apply an impulsive force at the free end of the beam (at x= 990 mm), and the force transducer signal and two accelerometer signals were sampled at a frequency of 2.56 kHz over a window of approximately 12.8 seconds. The sampling frequency provided measurements at 128 samples per cycle of the periodic orbit, and the time window allowed enough time for the perturbed response to decay until only the underlying periodic orbit remained. In order to determine the underlying periodic orbit and match its phase to that of the perturbed responses, the second half of the time histories, which consisted of only the periodic orbit, were used to find the true frequency of the periodic orbit based on a minimization search with MATLAB's 'fminsearch' function. This frequency was found to be 20.0000 Hz, and it was used to fit a multi-harmonic sinusoid to the periodic orbit (i.e. over the second half of the time histories). This fit can be used to recreate the periodic orbit over the entire time series (assuming that it is stationary). This process produces the underlying periodic orbit and assures that its phase is aligned with that of the underlying periodic orbit. The reconstructed periodic orbit, the perturbed response, and the difference between the two are plotted for the tip degree of freedom in Figure 16 with the same format that was used previously. The perturbation about the periodic orbit can clearly be seen in the early time response, since its relative magnitude is somewhat large compared to the periodic orbit magnitude. At late times the perturbed signal is almost indistinguishable from the periodic orbit. Note also that the periodic orbit is far from a pure sinusoid (as one would expect for a linear system). Several high frequency oscillations are present.
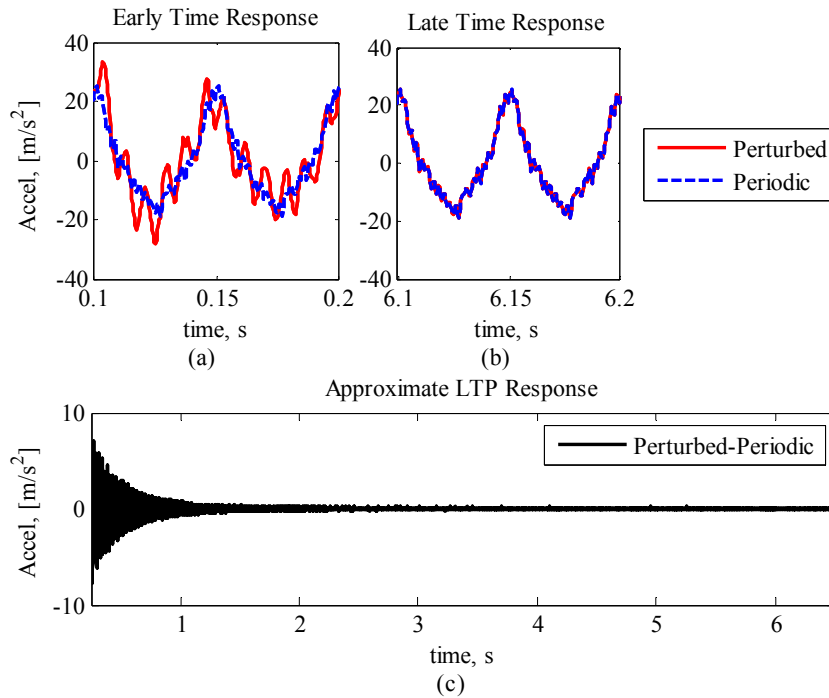
Fig. 16 Tip responses of the experimental beam for forcing frequency f_{exp}=20 Hz

The FFTs of the perturbed response and the perturbed minus the periodic responses were calculated, and those spectra are plotted in Figure 17 using the same format that was used previously. A number of sharp peaks occur in the perturbed response at 20 Hz and all of the harmonics of that frequency (i.e. 40, 60, 80 Hz, etc.) that are shown in the plots. Although the 20 Hz peak is the largest, the remaining peaks do not appear to diminish with increasing frequency. Since a single 20 Hz frequency sinusoid was used to force the system, this suggests that the system is highly nonlinear. There are many other artifacts that occur in the spectra, but a few coherent peaks can be seen at 28.2 and 188.2 Hz in (a) and (b) as well as 48.2 and 68.2 Hz in (b). A prominent peak occurs in both plots at 122.1 Hz, and two peaks of similar characteristics but much smaller magnitudes occur at 102.1 Hz and 162.2 Hz in plot (b). In each group of peaks previously listed, the peaks are separated by integer multiples of the scan frequency, and therefore are likely due to time-periodic effects.
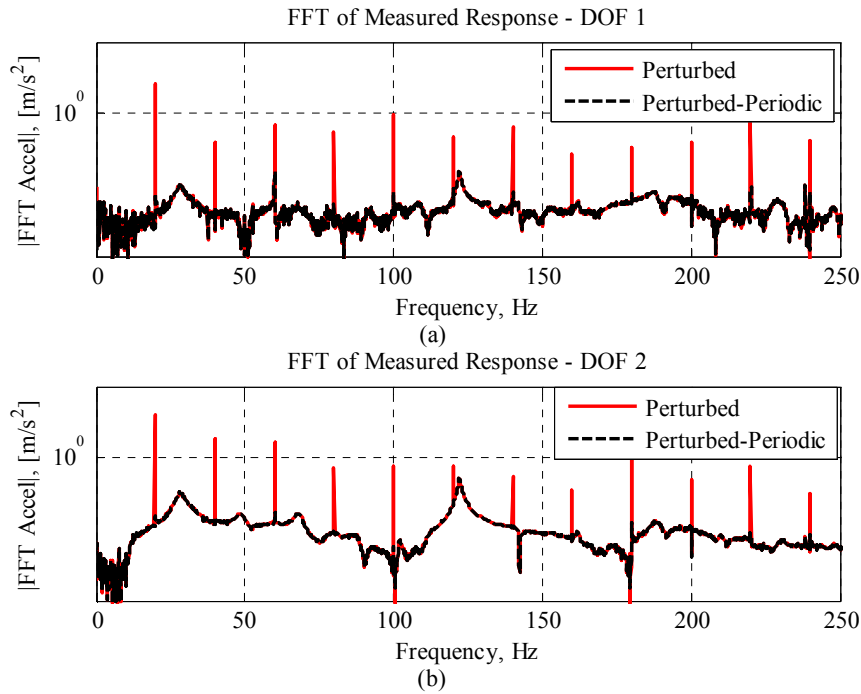
FFT of Measured Response - DOF 1

FFT of Measured Response - DOF 2

Fig. 17 Response spectra of the nonlinear beam measurements for forcing frequency f_{exp}=20 Hz

The peaks at 28.2 Hz and 122.2 Hz can be attributed to the m=0 harmonics of the two time-periodic modes of this system. The peaks at 48.2, 68.2, and 188.2 Hz can be attributed to m= +1, +2, and +8 harmonics of the former, and the peaks at 102.2 and 162.2 Hz can be seen as the m= -1 and +2 harmonics of the latter. The lifting method was applied to the perturbed minus periodic responses, and the FFT of the lifted responses was calculated. The composite spectrum of the lifted responses is plotted in Figure 18 with the solid black line. AMI identified two modes in the responses with eigenvalues λ_1= -2.777 +13.491i and λ_2= -6.966 +51.553i, natural frequencies $|\lambda_1|/(2\pi)$= 2.192 Hz and $|\lambda_2|/(2\pi)$=8.280 Hz, and damping ratios 0.2016 and 0.1339, respectively. The plot also shows the reconstruction of the composite spectrum based on the fit and the subtraction residual, which is significantly reduced by the two mode fit. This reveals that a linear-time periodic model fits the response of this highly nonlinear system very well about the limit cycle.
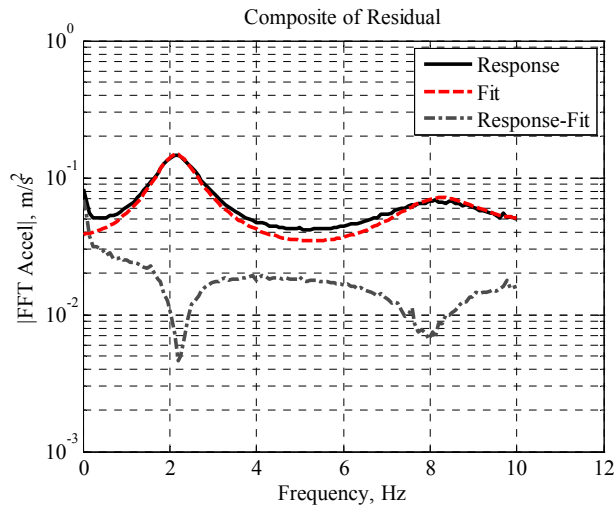

Fig. 18 Composite spectrum of lifted responses and AMI fit of the lifted responses for the nonlinear beam simulation for forcing frequency forcing frequency f_{exp}=20 Hz

The first eigenvalue can be deciphered to be an aliased version of the mode at 122.1, since 2.192 +6*20 = 122.192, and the second eigenvalue is the aliased version of the mode at 28.2 Hz, since 8.280+1*20 = 28.280. The time-periodic modes that

AMI extracted from the measurements were very noisy, so when they were expanded in a Fourier series, the previous information was used to retain only those harmonics that were clearly represented in the measurements. Different time varying state matrices would be obtained depending on which terms were retained in the model for the state transition matrix. To illustrate this, the state transition matrix and state coefficient matrix were constructed based on using one, two, and three Fourier terms for this system. The Fourier coefficients that were used to construct these models are defined in the legend for modes 1 (denoted m_1) and 2 (denoted m_2). The (3, 2) and (4, 2) coefficients of the resulting estimated state coefficient matrices are plotted in Figure 19. The estimated models with a single m=0 Fourier term have linear time-invariant coefficients, and as more terms are included in the expansion, the coefficients show increasing variation with time. With the three Fourier term model, the (3, 2) term of the state coefficient matrix varies by 85% of its minimum magnitude and the (4, 2) term varies by 30%.
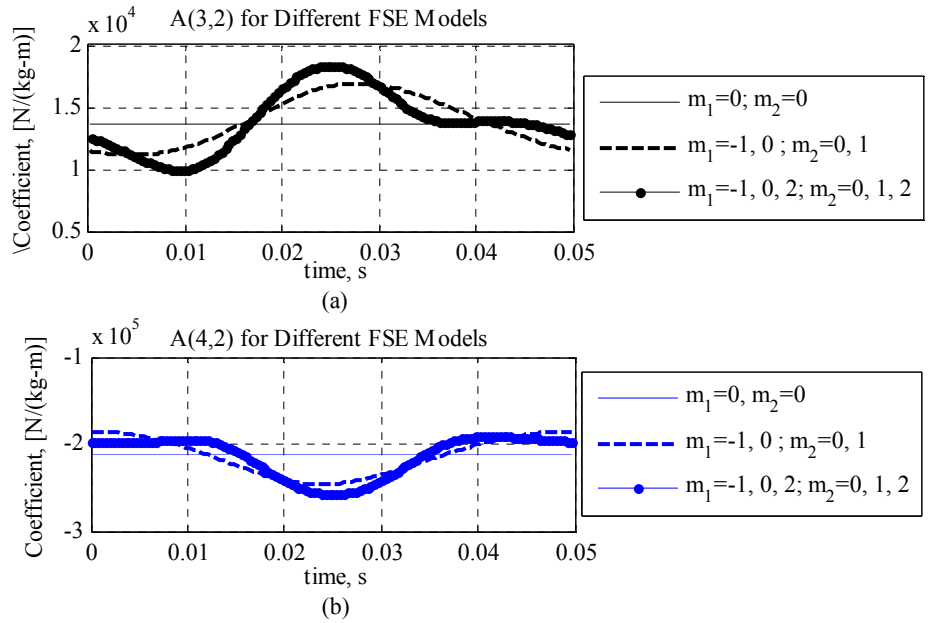

Fig. 19 Estimated time-periodic state coefficient matrix components for forcing frequency f_{exp}=20 Hz

The proposed identification method assumes that the system is oscillating in a stable periodic limit cycle. As mentioned previously, the limit cycle is measured by capturing the response of the system after the perturbation has decayed. The Fourier coefficients of the periodic limit cycle are then obtained and used in the analysis. Those Fourier coefficients are used to calculate the restoring forces using eq. (13), and also to compute the total restoring forces using eq. (15) as part of the validation step described in Section 2.2.5. The two measured acceleration signals and the measured force signal are plotted with blue dots in Figure 20. Each cycle of the assumed periodic response is overlaid, so the the time window shown corresponds to only one period of the steady state force and response. The Fourier series fit to each signal is also plotted with a solid red line. The acceleration of the beam's midspan (Accel 1) and tip (Accel 2) DOFs ranges between about ±10m/s^2 and ±40m/s^2, respectively. The input force ranges between about ±5 N. There is significant uncertainty due to noise in all three signals, yet each signal also seems to contain some high frequency fluctuations that are quite repeatable as well. These fluctuations are responsible for the high frequency harmonics seen in Figure 17. The harmonics describing the periodic orbit do not seem to diminish substantially in magnitude as frequency increases. Although it is not shown, these peaks are present at the integer multiples of the forcing frequency for the entire sampling bandwidth.
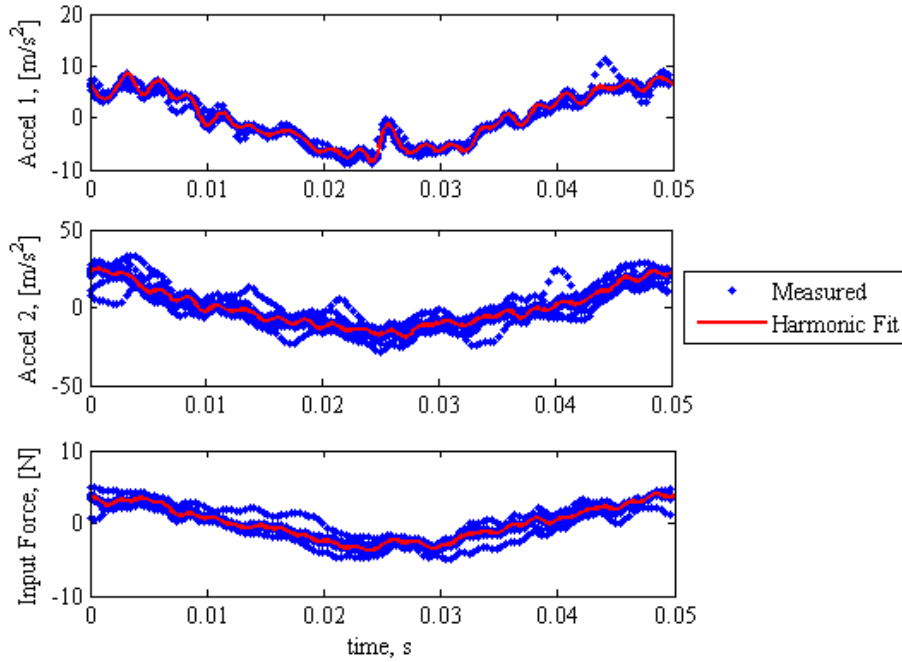
Fig. 20 Measured periodic signals and harmonic fits plotted period and overlaid for f_{exp}=20 Hz

Discussion

The signals plotted in the figure seem to indicate that the accelerations in this system fluctuate wildly over the limit cycle, especially at the midspan of the beam. Hence, many harmonics are needed to define the periodic limit cycle, and so one would expect that the linear time-periodic model of the system about this limit cycle must also contain many harmonic terms. Although linear time-periodic behavior was clearly visible in the experimental measurements, only a few harmonics were discernible from the noise, so a trustworthy estimate of the $A(t)$ matrix could not be obtained. In any event, the accuracy with which the limit cycle is known seems questionable, so any measure of the dynamics about that limit cycle would have limited value. It seems that more care must be taken to obtain a valid limit cycle before the proposed system identification technique can be applied to this system. It would also be preferable to have a limit cycle that is described by a smaller number of harmonics. Furthermore, i this work we have proposed to validate the nonlinear model identified by linear time-periodic identification using the restoring force surface method, but that method was also found to give meaningless results due to the fluctuations in the measured accelerations and input force. Future works will seek to refine the test methodology to produce more reliable measurements in order to address these issues. Even then, it is also interesting to note that very clear linear time-periodic behavior was visible in this system's response (e.g. Figures 17 and 18), even though the measurements were not of sufficient quality to allow that behavior to be related to the system's nonlinear equation of motion.

4. Conclusions

This work explores a new system identification strategy for nonlinear systems that is based on approximating the system's dynamics as linear time-periodic about a stable limit cycle. A variant of the restoring force surface method was proposed that estimates the total restoring forces in the system over the periodic orbit, which can be helpful in validating the nonlinear model found by the linear time-periodic identification approach. The approach was applied to simulated measurements from a two DOF cantilever beam and found to be capable of identifying the force-displacement relationships in the system from simulated measurements. However, the damping forces were not accurately estimated and the method was sensitive to the number of terms used in the state transition matrix of the linear time-periodic model. Even then, it is significant that the method identifies the nonlinear force displacement relationships in the system without any a priori assumption regarding the form of the nonlinearity or the order of the system. Two different excitation strategies were explored, which illustrated that it is important to choose an excitation that strongly activates the nonlinear parameters over a large range of motion in order to observe the nonlinearity. Additionally, the simulations revealed that it was important to assure that the perturbation from the underlying periodic orbit was small enough so that it could be modeled as linear time-periodic.

The methods were also applied to experimental measurements from a nonlinear beam with a geometric nonlinearity at its tip. Measurements from this system showed clear signs of time-periodic behavior. However, the system was found to deviate significantly from the periodic limit cycle and that cycle itself was not very repeatable, so neither the proposed linear time-periodic identification method nor the restoring force surface method gave reasonable results. The authors are presently studying this issue and mapping the periodic orbits that are possible (see [22]) to better understand how to best apply the proposed identification methodology to experimental measurements from high order systems.

5. References

[1]   G. Dimitriadis and J. Li, "Bifurcation of Airfoil Undergoing Stall Flutter Oscillations in Low-Speed Wind Tunnel," *AIAA Journal,* vol. 47, pp. 2577-2596, 2009.

[2]   G. T. Flowers*, et al.*, "The Application of Floquet Methods in the Analyses of Rotordynamic Systems," *Journal of Sound and Vibration,* vol. 218, pp. 249-259, 1998.

[3]   C. Basdogan and F. M. L. Amirouche, "Nonlinear Dynamics of Human Locomotion: From the Perspective of Dynamical Systems Theory.," in *Engineering Systems Design and Analysis Conference*, 1996.

[4]   J. B. Dingwell and J. P. Cusumano, "Nonlinear time series analysis of normal and pathological human walking," *Chaos,* vol. 10, pp. 848-63, 2000.

[5]   R. F. Ker*, et al.*, "The Spring in the Arch of the Human Foot," *Nature,* vol. 325, pp. 147-149, 1987.

[6]   R. A. Heath*, et al.*, "Detecting Nonlinearity in Psychological Data: Techniques and Applications," *Behavior Research Methods, Instruments, & Computers,* vol. 32, pp. 280-289, 2000.

[7]   C. Georges and J. C. Wallace, "Learning Dynamics and Nonlinear Misspecification in an Artificial Financial Market," *Macroeconomic Dynamics,* vol. 13, pp. 625-655, 2009.

[8]   S. F. Masri and T. K. Caughey, "A Nonparametric Identification Technique for Nonlinear Dynamic Problems," *Journal of Applied Mechanics,* vol. 46, pp. 433-447, 1979.

[9]   D. Donnelly and E. Rogers, "Time Series Analysis with the Hilbert-Huang Transform," *American Journal of Physics,* vol. 77, pp. 1154-1161, 2009.

[10]   G. Kerschen*, et al.*, "Past, Present and Future of Nonlinear System Identification in Structural Dynamics," *Mechanical Systems and Signal Processing,* vol. 20, pp. 505-592, 2006.

[11]   G. Kerschen, Kowtko, J., McFarland, D.M., Bergman, L., Vakakis, A., "Theoretical and Experimental Study of Multimodal Targeted Energy Transfer in a System of Coupled Oscillators," *Nonlinear Dynamics,* vol. 47, pp. 285-309, 2007.

[12]   M. S. Allen and M. W. Sracic, "System Identification of Dynamic Systems with Cubic Nonlinearities Using Linear Time-Periodic Approximations," presented at the ASME International Design Engineering Technical Conferences & Computers and Information in Engineering Conference, San Diego, California, USA, 2009.

[13]   M. S. Allen, "Frequency-Domain Identification of Linear Time-Periodic Systems Using LTI Techniques," *Journal of Computational and Nonlinear Dynamics,* vol. 4, pp. 041004.1-041004.6, 2009.

[14]   M. W. Sracic and M. S. Allen, "Method for Identifying Models of Nonlinear Systems Using Linear Time Periodic Approximations," *Mechanical Systems and Signal Processing,* vol. Submitted, 2010.

[15]   G. Floquet, "Sur Les Equations Lineairs a Coefficients Periodiques," *Ann. Sci. Ecole Norm. Sup.,* vol. 12, pp. 47-88, 1883.

[16]   P. Arambel and G. Tadmor, "Robust H_∞ Identification of Linear Periodic Discrete-Time Systems," *International Journal of Robust and Nonlinear Controol,* vol. 4, pp. 595-612, 1994.

[17]   P. Friedmann and C. E. Hammond, "Efficient Numerical Treatment of Periodic Systems with Application to Stability Problems," *International Journal for Numerical Methods in Engineering,* vol. 11, pp. 1117-1136, 1977.

[18]   F. Thouverez, "Presentation of the ECL Benchmark," *Mechanical Systems and Signal Processing,* vol. 17, pp. 195-202, 2003.

[19]   G. Kerschen, Lenaerts, V., Golinval, J.C., "Identification of a Continuous Structure with a Geometrical Non-Linearity. Part I: Conditioned Reverse Path Method," *Journal of Sound and Vibration,* vol. 262, pp. 889-906, 2003.

[20]   K. Worden and G. R. Tomlinson, "A Review of Nonlinear Dynamics Applications to Structural Health Monitoring," *Strucrural Control and Health Monitoring,* vol. 15, pp. 540-567, 2007.

[21]   J. H. Ginsberg, *Mechanical and Structural Vibrations Theory and Applications*, 1 ed. New York: John Wiley & Sons, Inc., 2001.

[22]   M. W. Sracic and M. S. Allen, "Numerical Continuation of Periodic Orbits for Harmonically Forced Nonlinear Systems," presented at the 29th International Modal Analysis Conference (IMAC XXVI), Jacksonville, Florida, USA, 2011.

[23]   M. S. Allen and J. H. Ginsberg, "A Global, Single-Input-Multi-Output (SIMO) Implementation of The Algorithm of Mode Isolation and Applications to Analytical and Experimental Data," *Mechanical Systems and Signal Processing,* vol. 20, pp. 1090–1111, 2006.
[24]   M. S. Allen and M. W. Sracic, "A New Method for Processing Impact Excited Continuous-Scan Laser Doppler Vibrometer Measurements," *Mechanical Systems and Signal Processing,* vol. 24, pp. 721-735, 2010.
[25]   A. H. Nayfeh and D. T. Mook, *Nonlinear Oscillations*. New York: John Wiley and Sons, 1979.
[26]   R. L. Mayes and A. J. Gomez. (2006) What's Shakin', Dude? Effective Use of Modal Shakers. *Experimental Techniques*. 51-61.

 Appendix

The spring steel on the tip of the beam acts as a tension on element, and transfers force by its line of action which is assumed to always be straight. When the beam tip is deflected by a small amount δ, then so is the spring steel element, and it forms a small angle with the right support, θ. A diagram of this geometry is shown in Figure **21**.   The spring steel which had original length l_s is assumed to strain by an amount Δl_s due the tension force F in the element. By the force displacement relationship of a tensile element, $\Delta l_s = F l_s/(E_s A_s)$ where E_s is the elastic modulus of the spring steel and A_s is the cross section area of the strip. Therefore, the tensile force is $F = E_s A_s/l_s * \Delta l_s$. Next, the strain can be related to the geometry of the tip deflection.
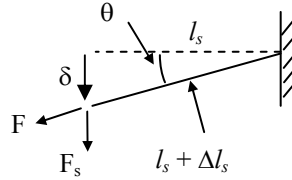

Fig. 21 Geometry for beam tip deflection and interaction of the strip of spring steel

The tip of the beam has a deflection of δ, which can be used to write the strain in the spring steel as a function of the undeformed length.

$$\Delta l_s = \sqrt{l_s^2 + \delta^2} - l_s \tag{24}$$

The vertical contribution of the tensile force is $F_v = F \sin(\theta)$, or using the geometry of the figure and the previous relationship,

$$F_v = \frac{E_s A_s}{l_s}\left(\sqrt{l_s^2 + \delta^2} - l_s\right)\left(\frac{\delta}{l_s + \sqrt{l_s^2 + \delta^2} - l_s}\right) = \frac{E_s A_s}{l_s}\left(\delta - l_s \delta \left(l_s^2 + \delta^2\right)^{1/2}\right) \tag{25}$$

In order approximate the vertical force displacement relationship about small tip deflections of the beam, the previous equation was expanded in a Taylor series about $\delta=0$ for terms to $O(\delta^3)$, and the higher order terms were neglected. This results in the following expression for the vertical force contribution of the spring steel.

$$F_v \cong \frac{E_s A_s}{2 l_s^3} \delta^3 \tag{26}$$

The nonlinear spring constant can therefore be approximated as $k_3 = E_s A_s/(2 l_s^3)$.